

Modelling compression ignition engines by incorporation of the flamelet generated manifolds combustion closure

Amin Maghbouli, Berşan Akkurt, Tommaso Lucchini, Gianluca D'Errico, Niels G. Deen & Bart Somers

To cite this article: Amin Maghbouli, Berşan Akkurt, Tommaso Lucchini, Gianluca D'Errico, Niels G. Deen & Bart Somers (2018): Modelling compression ignition engines by incorporation of the flamelet generated manifolds combustion closure, Combustion Theory and Modelling, DOI: [10.1080/13647830.2018.1537522](https://doi.org/10.1080/13647830.2018.1537522)

To link to this article: <https://doi.org/10.1080/13647830.2018.1537522>



© 2018 The Author(s). Published by Informa UK Limited, trading as Taylor & Francis Group.



Published online: 24 Oct 2018.



Submit your article to this journal [↗](#)



Article views: 220



View Crossmark data [↗](#)



Modelling compression ignition engines by incorporation of the flamelet generated manifolds combustion closure

Amin Maghbouli^{a*}, Berşan Akkurt^a, Tommaso Lucchini^b, Gianluca D'Errico^b,
Niels G. Deen^a and Bart Somers^a

^aMultiphase and Reactive Flows Group, Department of Mechanical Engineering, Eindhoven University of Technology, Eindhoven, Netherlands; ^bInternal Combustion Engine Group, Energy Department, Politecnico di Milano, Milan, Italy

(Received 19 March 2018; accepted 4 October 2018)

Tabulated chemistry models allow to include detailed chemistry effects at low cost in numerical simulations of reactive flows. Characteristics of the reactive fluid flows are described by a reduced set of parameters that are representative of the flame structure at small scales so-called *flamelets*. For a specific turbulent combustion configuration, flamelet combustion closure, with proper formulation of the flame structure can be applied. In this study, flamelet generated manifolds (FGM) combustion closure with progress variable approach were incorporated with OpenFOAM[®] source code to model combustion within compression ignition engines. For IC engine applications, multi-dimensional flamelet look-up tables for counter flow diffusive flame configuration were generated. Source terms of non-premixed combustion configuration in flamelet domain were tabulated based on *pressure, temperature of unburned mixture, mixture fraction, and progress variable*. A new frozen flamelet method was introduced to link one dimensional reaction diffusion space to multi-dimensional Computational Fluid Dynamics (CFD) physical space to fulfill correct modelling of thermal state of the engine at expansion stroke when charge composition was changed after combustion and reaction rates were subsided. Predictability of the developed numerical framework were evaluated for Sandia Spray A (constant volume vessel), Spray B (light duty optical Diesel engine), and a heavy duty Diesel engine experiments under Reynolds averaged Navier Stokes turbulence formulation. Results showed that application of multi-dimensional FGM combustion closure can comprehensively predict key parameters such as: *ignition delay, in-cylinder pressure, apparent heat release rate, flame lift-off*, and *flame structure* in Diesel engines.

Keywords: flamelet generated manifolds; tabulated chemistry; diesel engines; open-FOAM

1. Introduction to tabulated chemistry

Today combustion of reactive spray systems such as industrial burners, jet engine combustors, or internal combustion engines are contributing a lot to our power demand as well as emitted emissions [1]. The combustion process is influenced by the complex interplay of the liquid fuel spray evolution, turbulent fluid flow, and chemical reactions. Reproducible

*Corresponding author. Email: a.maghbouli@tue.nl

experiments are required to better understand the involved interacting physical phenomena. Parallel to the experimental efforts and driven by the need to reduce pollutant emissions (NO_x and soot) while simultaneously maintaining high efficiencies, comprehensive and accurate numerical methods are of great importance for the further development and optimisation of the reactive spray configurations. Within this context, the engine combustion network (ECN) promotes collaborations among researchers and makes a large set of experimental data publicly available [2]. For Diesel combustion, attention has mainly focused on the so-called *Spray A* configuration, where *n*-dodecane fuel is delivered by a single hole nozzle in a constant volume chamber at ambient conditions similar to those encountered in engines at the start of injection (SOI) [3–6]. The experimental database includes non-reacting and reacting conditions at variable ambient temperature (300–1400 K), density (3.8–22.8 kg/m³), injection pressure (30–150 MPa) and Oxygen concentration (0–21%) [2]. Also from ECN 4 there is an additional section of *Spray B* which is application of Spray A injector in an optical Diesel engine. Experiments such as Spray A and Spray B are necessary for application of emerging new fuels, fuel additives, and modern engine combustion modes such as (Low Temperature Combustion) LTC in automotive industries in one hand and more intensified need for detailed understanding of auto-ignition and combustion for optimisation purposes on the other. This resulted in a high interest on comprehensive application of detailed reaction mechanisms within multi-dimensional CFD [7,8]. Nevertheless, such a methodology in reactive flow simulations results in a high demand for computational power due to the highly nonlinear behaviour of the chemical kinetics mechanisms. In case of IC engines this is more pronounced as much larger computational domains are needed.

Rutland [9] discussed that performing the large Eddy simulations (LES) for IC engine applications require enhancement of combustion models in terms of accuracy and affordable computational time. It was also discussed that such developments for the combustion models should be first successfully applied to the Reynolds averaged Navier Stokes (RANS) formulation as computational capacity largely increases by applying LES. Over the years, different concepts were introduced to reduce CPU time dedicated to chemistry calculations. Some dealing with mechanism reduction aspects of the chemical kinetics mechanisms such as dynamic adaptive chemistry [10], and *in situ* adaptive tabulation [11] and others dealing with more efficient manipulation of chemistry in the framework of conservation equations such as multi-zone chemistry model which instead of integrating chemistry for each computational cell, solves it in clusters of CFD cells grouped by predefined criteria [12,13]. Tabulated chemistry is an alternative way to include chemical kinetics mechanism with noticeably lower computational costs. The main difference is that combustion source terms in the conservation equations were not calculated while solving for CFD and instead, change in thermal state of the reacting mixture in a time-step is read and updated from previously generated tables using a transported scalar so-called *progress variable*. In this context, the progress variable is the link between fluid flow calculation and tabulated chemistry (flamelet look-up tables) and needs a comprehensive definition, transport, retrieval, and utilisation. Failure in any of the mentioned characteristics of the progress variable, will result in wrong determination of thermal state of reactive fluid flow. Definition and utilisation of the progress variable is not unique, however, as Ihme *et al.* [14] stated, the choice of a suitable progress variable should be guided by the following principles: (a) Being able to be transported within CFD domain. (b) The reactive scalars used for its definition, should all evolve on comparable time scales. (c) Generation of flamelet tables should be based on independent parameters. and (d) Mentioned independent parameters

should uniquely characterise one point in the thermochemical state-space. There have been different methodologies on generation of the flamelet tables such as: flamelet generated manifolds (FGM) [15,16], flamelet prolongation of ILDM (FPI) [17,18], and homogeneous reactor (HR) [19–22].

Although all mentioned combustion closures were applied to model constant volume vessel experiments such as Spray A by different researchers [6,23–26], there are very rare publications on their application within IC engines simulations. Lehtiniemi *et al.* [27] applied representative interactive flamelet (RIF)-based tabulation method to model Diesel engines. They used steady flamelet calculations fed into unsteady flamelet solvers to tabulate progress variable and desired parameters, however, their flamelet and table generation took six months to be used later in engine CFD calculations. Also their engine CFD simulation was not extensively evaluated with the experiments. Bekdemir *et al.* [16] applied FGM in the STAR-CD commercial software to model *n*-heptane spray combustion in a Diesel engine. They concluded that more than three pressure levels for flamelet tables are needed to obtain comparable results to the experiments. Nevertheless, their simulation results showed unphysical pressure rise rate (PRR) by any number of pressure levels applied. Egüz *et al.* [28] used FGM combustion closure on modelling Partially Premixed Compression Ignition (PPCI) engines. They concluded that lower strain rate for flamelet generation provides better results for PPCI configuration. However, CFD results showed very high heat release and PRRs for their methodology of flamelet generation. Recently, Lucchini *et al.* [21] applied HR tabulation methods to model Diesel engines. They obtained good agreements with the experimental results for a large range of experimental parameters, however, their combustion closure based on HR had strong assumption for rich mixture fractions where it was cut after certain yet reactive fuel flammability limits. Also Kundu *et al.* [29] applied flamelet residence time in table generation instead of progress variable. They reported promising result for a temperature sweep of ECN Spray A configuration as well as an optical engine case. Although this methodology avoids use of progress variable, CFD results were dependent on the number of needed flamelets to obtain reasonable residence times for different configurations.

As discussed, researchers over the years applied variety of tabulation methods to minimise computational overhead introduced by applying detailed chemical mechanisms. Majority of them focused on modelling and validation on constant volume configurations such as ECN Spray A. Unfortunately, number of available literature dramatically drops for real engine applications. To the authors knowledge, using tabulated chemistry, there was no specific attention given to proper modelling and verification of chemistry after main combustion stage and late cycle times. Although without reasoning, only Lehtiniemi *et al.* [27] discussed about the need to create low temperature flamelets in IC engine applications. This is because unlike constant volume vessels, global temperature in engines decreases due to expansion. Absence of the low temperature flamelets while tabulating chemistry will result in overestimation of mixture reactivity after top dead centre as well as thermal state of the engine while expansion. The main objective of this paper is to employ tabulated flamelets in the form of FGM combustion closure under RANS formulation to comprehensively predict ignition and combustion of Diesel sprays in constant volume vessel, light duty, and heavy duty engines. In order to properly model reactivity and thermal state of the engine after top dead centre, a novel frozen flamelet method (FFM) will be introduced and applied in engine configurations. Specific attention was given to tangibly reduce simulation times for flamelet generation, tabulation, and engine CFD calculations. Characteristics of transient liquid fuel spray from ignition to fully established diffusive

flame will be presented. Contents of this paper is the followings. The applied combustion closure with FGM will be discussed in Section 2.1. Implementation of FGM-based source and solver codes together with generation and tabulation of flamelets will be given in Section 2.2. Flamelet results will be discussed in Section 3 and the new FFM method will be explained in Section 4.2.4. Sections 4.1–4.3 will evaluate capabilities of the developed numerical framework for *Spray A*, *Spray B*, and *Sandia optical engine* configurations. Finally, concluding remarks will be summarised in Section 5.

2. Numerical modelling

Numerical modelling of the internal combustion engines is a multidisciplinary task involving a large number of physical and chemical phenomena. This is why a set of well interacting sub-models such as: moving grid management and boundary conditions, heat transfer, turbulence, liquid spray injection, break-up, vaporisation, air-fuel mixing, combustion, and emission are needed. In this paper the focus was given on the combustion closure. To read more about the other sub-models the reader can refer to [13,30,31].

2.1. FGM combustion closure

FGM approach is based on the widely used and accepted *flamelet* concept [32] and assumes that a high-dimensional thermal state space of reacting chemical species can be approximated by a low-dimensional manifold [33]. Difference between FGM-based combustion closure with classical RIF models which operate with on-the-fly chemistry is on storing and retrieval of the needed source terms in conservation equations. Main advantage is effectively reducing the CFD simulation times which is in high importance for IC engine calculations. To tackle modelling of non-premixed combustion, counter flow diffusion flames, the opposing fuel and oxidiser jets form a reaction zone close to the stagnation plane, can be considered [34]. One dimensional unsteady flamelet equations are given by:

$$\frac{\partial \rho}{\partial t} + \frac{\partial \rho u}{\rho x} = -\rho K, \quad (1)$$

$$\frac{\partial \rho Y_n}{\partial t} + \frac{\partial \rho u Y_n}{\rho x} = \frac{\partial}{\partial x} \left(\rho D \frac{\partial Y_n}{\partial x} \right) + \dot{\omega}_n - \rho K Y_n, \quad (2)$$

$$\frac{\partial \rho h}{\partial t} + \frac{\partial \rho u h}{\rho x} = \frac{\partial}{\partial x} \left(\frac{\lambda}{c_p} \frac{\partial h}{\partial x} \right) - \rho K h, \quad (3)$$

where D denoted as diffusion coefficient, u is one dimensional velocity in flamelet domain, ρ is density, Y_n is mass fraction of n^{th} specie in the chemical kinetics mechanism, K is stretch rate, $\dot{\omega}_n$ is molar production/destruction rate of n^{th} specie, h is enthalpy, λ is thermal conductivity, and c_p is specific heat. If flamelet look-up tables were generated based on equations above still it will be needed to link reaction space calculations with fluid flow simulations in CFD. This is done by a scalar so-called progress variable. Equation (4) is for transport of progress variable, denoted with C , within CFD domain (physical space).

$$\frac{\partial \rho C}{\partial t} + \frac{\partial \rho u C}{\rho x} = \frac{\partial}{\partial x} \left(\frac{\mu_t}{Sc_t} \frac{\partial C}{\partial x} \right) + \rho \dot{C}, \quad (4)$$

where μ_t and Sc_t are turbulent viscosity and Schmidt number and \dot{C} is source term of progress variable.

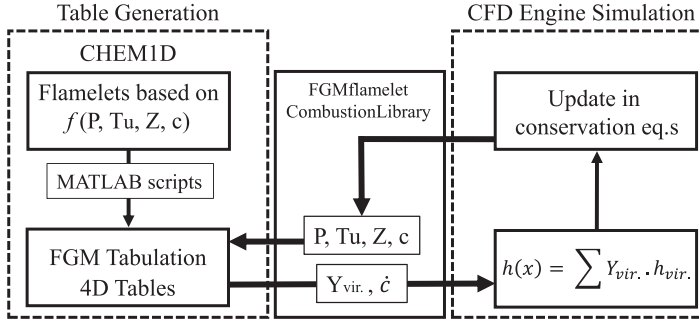


Figure 1. Schematic representation of connection between reaction and physical space, scripts, source, and solver codes for incorporation of FGM combustion closure to openFOAM CFD calculations (colour online).

Ignition and combustion of non-premixed or partially premixed configurations such as Diesel engines cannot be determined solely with the progress variable. Mixture fraction needs to be considered as an additional dimension for flamelet tabulation due to the mixing of the fuel with surrounding air. Equation (5) represents mixture fraction transport in physical space.

$$\frac{\partial \rho Z}{\partial t} + \frac{\partial \rho u Z}{\rho x} = \frac{\partial}{\partial x} \left(\mu_t \frac{\partial Z}{\partial x} \right) + \dot{S}_{\text{spray}}, \quad (5)$$

where Z is mixture fraction and \dot{S}_{spray} is source term due to the liquid spray.

2.2. Numerical implementation

In order to apply the FGM combustion closure, prior to reactive spray calculations, multi dimensional flamelet tables were generated. Equations (1) –(3) were utilised to model opposing fuel and oxidiser jets. For this purpose *CHEMID* a one dimensional flame code developed at the Eindhoven University of Technology [35,36] was used. Figure 1 shows the connection between reaction and physical spaces and the developed scripts, source, and solver codes.

Pressure, p , and unburned temperature, T_u , were included as additional table dimensions to progress variable, c , and mixture fraction, Z . Using such a representation, the thermal state of a reacting spray, ϕ , is expressed as $\phi = \mathcal{F}_\phi(p, T_u, Z, c)$ where \mathcal{F}_ϕ is the corresponding value from the flamelet solution. Details of flamelet table generation and their results will be discussed in Section 3. Generating flamelets for increased number of FGM table dimensions can result in a massive computational time overhead as reported by [27]. To tackle this issue two approaches were considered in this study:

(1) Instead of tabulating source terms of all participated chemical species in the applied chemical kinetics mechanism, seven *virtual specie* compositions were tabulated. Unburned gas temperature determined from enthalpy transport equation, Equation (6) to access the correct table entry and retrieve \dot{C} for closure of progress variable transport equation (Equation (4)).

$$\frac{\partial \rho h_u}{\partial t} + \frac{\partial \rho u h_u}{\rho x} = \frac{\partial}{\partial x} \left(\alpha_t \frac{\partial h_u}{\partial x} \right) + \frac{\rho}{\rho_u} \cdot \frac{Dp}{Dt}, \quad (6)$$

where h_u is unburned enthalpy, α_t is turbulent thermal diffusivity, and ρ_u is unburned gas density. The virtual species approach was presented and validated by the authors. For more explanations of this approach reader can refer to [21,31,37].

(2) *bash* scripts were developed to solve flamelets in parallel CPU cores. These scripts set up flamelet initial and boundary conditions for specified intervals of pressure and unburned gas temperatures and then CHEM1D was run in multiple cores.

After flamelet table generation, developed MATLAB scripts will create data arrays to be used later in CFD. A new class of *FGMflameletCombustionLibrary* was implemented to Lib-ICE and OpenFOAM source codes. For the FGM combustion closure, this class will handle allocation on retrieval of \dot{C} and virtual species compositions. As Figure 1 shows, *FGMflameletCombustionLibrary* receives values of p , T_u , Z , and c of a computational cell from the CFD solver and passes them to the look-up routine which will return new virtual species composition and \dot{C} . Former will be used to update energy transport in the form of enthalpy and latter will update transport of progress variable.

The definition of the progress variable in the FGM tables was based on linear combination of specified chemical species as represented below:

$$C = Y_{\text{HO}_2} + Y_{\text{CH}_2\text{O}} + Y_{\text{H}_2\text{O}} + Y_{\text{CO}_2} + Y_{\text{CO}}. \quad (7)$$

Selection of these chemical species fulfilled a monotonic increase of the progress variable and at the same time effectively represents combustion phasing of a reacting spray from onset of ignition to fully established diffusion flame. MATLAB scripts then determine progress variable reaction rates and chemical composition as a function of the discrete values of the *normalised progress variable*, c :

$$c = \frac{C - C_{\min}}{C_{\max} - C_{\min}}, \quad (8)$$

where C_{\min} and C_{\max} are the minimum and maximum values of the progress variable found before and after ignition of flamelet calculations. Normalised progress variable later will only be needed for look-up routines and correct retrieval of the updating parameters.

3. Flamelet results

Flamelet calculations were conducted for the opposing fuel and oxidiser jets as schematically shown in Figure 2(a). The chemical kinetics mechanism reduced by Yao *et al.* [38], which was validated for reactive spray simulations, was used for oxidation chemistry of *n*-dodecane throughout this study. Properties of baseline Spray A operating condition of 900 K, 15% O₂, 22.8 kg/m³ [2] were initialised in the flamelet simulations with a single flame strain rate of 500 s⁻¹ and resulting flame structure diagram can be seen in Figure 2(b). Selection of a single value of 500 s⁻¹ strain rate was based on ignition delay analysis conducted in [26,39,40] for different strain rates. It has been found that for Spray A configuration, ignition delay time is almost insensitive for strain rates less than 1000 s⁻¹. Figure 2(b) shows that unsteady igniting flamelets were started from lean mixture fractions, burned rich mixture fractions, and returned and stabilised on stoichiometric mixture fraction, Z_{St} , with the highest burning temperature forming thermal equilibrium lines.

Flamelet generation results for oxidiser temperatures of 800 K, 900 K, and 1000 K all with constant pressure of 60 bar were compared in Figure 3 where progress variable was

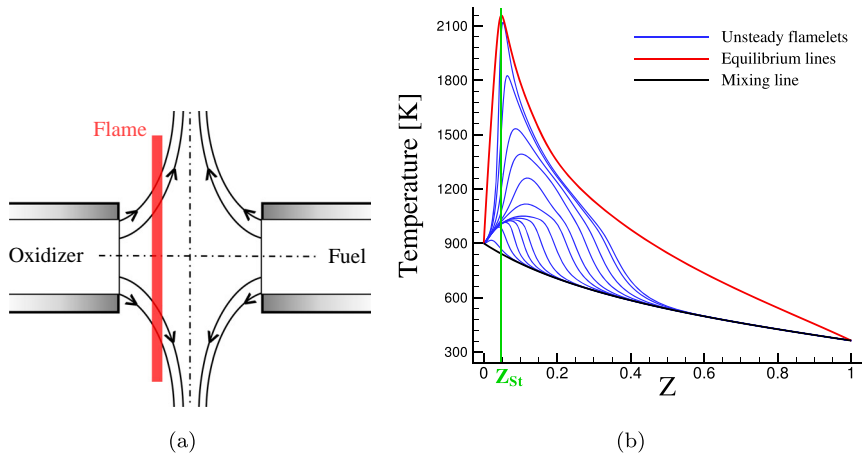


Figure 2. (a) Schematic representation of opposing fuel and oxidiser jets and diffusive flame location and (b) Unsteady flamelet simulation results of mixture fraction versus temperature for the strain rate of 500 s^{-1} . *n*-dodecane fuel counter flow configuration to represent Spray A baseline operating condition: 900 K, 15% O_2 , 22.8 kg/m^3 (colour online).

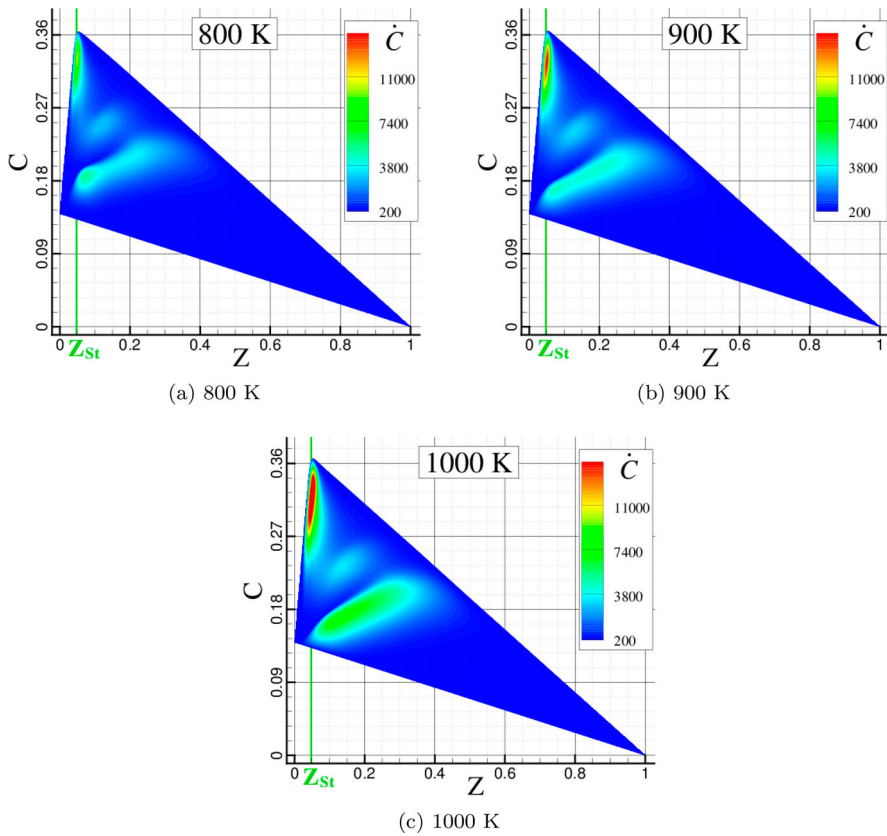


Figure 3. Contours for rate of progress variable as function of mixture fraction and progress variable for Spray A ambient temperatures of 800 K, 900 K(baseline), and 1000 K (colour online).

plotted versus mixture fraction and coloured by the rate of progress variable. Firstly, due to the applied chemical species in the definition of the progress variable in Equation (7) and presence of CO_2 and H_2O in Spray A ambient oxidiser composition, progress variable has a value at $Z=0$ and reaches zero at $Z=1$. Secondly, higher progress variable sources (lower green regions) start from slightly leaner mixture fractions for all ambient temperatures and reach rich mixture fractions and finally the maximum value at Z_{St} . It can be seen that by increasing the ambient temperature, higher reaction rates occurred and the maximum progress variable rate was higher in 1000 K compared to that of baseline case. Once the flamelets are generated they can be used in needed format in CFD applications. Characteristics of flamelet generation and their tabulation for specific cases will be discussed in the next section.

4. Case description

Three different configurations of reacting sprays will be discussed in this section. As mentioned before, flamelet calculations and FGM table generations are conducted with CHEM1D and the developed MATLAB scripts. However, in order to minimise needed computational memory while reading an FGM table, dimensions and table resolutions are case dependent. Properties of FGM tables for each case are presented separately.

4.1. Constant volume vessel experiments | ECN: Spray A

Experimental studies on Spray A configuration were conducted and still continuing mainly in Sandia National Laboratories, Eindhoven University of Technology, IFPEN, and CMT-Motores. Sandia's experimental apparatus is briefly discussed here. More information is available on the ECN pages [2].

The Sandia set-up is an optically accessible, constant-volume, cubic combustion vessel. Its total volume is 1147 cm^3 . The injector is a very close representative of those used in common-rail, direct-injection Diesel engines and is located at the centre of one face of the chamber. Two spark plugs and a mixing fan are mounted for ignition (providing high ambient temperature) and homogenising the mixture before the spray, respectively. A wide range of ambient conditions, i.e. different temperature, density, oxidiser ratio, and injection pressure similar to conditions at injection in Diesel engines were provided. For sufficiently long injection duration, a lifted turbulent spray flame is formed. Low/high ambient temperatures, pressures, and densities correspond to early/late injection strategies in an engine, respectively, and different levels of EGR are simulated using different ambient oxygen concentrations. Measurements are available for several single and multi-component fuels, including both hydrocarbons and oxygenated fuels. The injector is a single-orifice, axial injector nozzle of the mini-sac type tip with a top-hat injection profile. Table 1 summarises specifications of the baseline Spray A experiments.

4.1.1. Non-reacting spray results

Taking advantage of symmetry for Sandia's constant volume vessel of Spray A experiments, a two dimensional wedge grid is generated. Grid is finer on the injection axis and coarser on the parts of the domain which is not affected by spray. A grid and spray sub-model dependency study for liquid n-dodecane injection can be found in [31]. For the non-reactive simulations, the temperature of the internal mixture was set to 900 K

Table 1. Specifications for Spray A baseline operating condition of the ECN [2].

Ambient gas temperature	900 K
Ambient gas pressure	≈ 6.0 MPa
Ambient gas density	22.8 kg/m^3
Ambient gas oxygen (Vol)	15% O_2 (reacting); 0% O_2 (non-reacting)
Ambient gas velocity	Near-quiescent, < 1 m/s
Fuel injector	Bosch solenoid-activated
Injector nominal nozzle outlet diameter	0.090 mm
Nozzle K factor	1.5
Discharge coefficient	$C_d = 0.86$
Number of holes	1 (single hole)
Orifice orientation	Axial (0° full included angle)
Fuel injection pressure	150 MPa (1500 bar)
Fuel	<i>n</i> -dodecane
Fuel temperature at nozzle	363 K
Injection duration	1.5 ms
Injection mass	3.5 – 3.7 mg

Table 2. Summary of applied sub-models on diesel spray simulations in this study.

Modelling of	Applied models
Turbulence	Standard $k - \epsilon$
Injection	Huh injector
Spray atomisation	Huh–Gosman
Spray breakup	KHRT
Spray evaporation	Spalding
Droplet heat transfer	Ranz Marshall

and pressure to 60 bar. Mass fractions of the initial species are: $Y_{O_2} = 0$, $Y_{N_2} = 0.884$, $Y_{H_2O} = 0.022$, and $Y_{CO_2} = 0.094$. The total injected mass was 3.5 mg and injection profile was taken from the experimental database of Spray A in [2]. Summary of applied sub-models for the spray simulation and turbulence are presented in Table 2. Based on ECN recommendations for modelling turbulence in reacting sprays, C_1 constant of $k - \epsilon$ model was set to the value of 1.54.

Liquid and vapour penetration lengths were extracted from numerical simulations and are compared to ECN Spray A experimental data in Figure 4. For explanations of applied thresholds for liquid and vapour penetrations refer to [13]. Moreover, mixture fraction distribution contour for the steady state spray at 0.75 ms is compared to the experimental data in Figure 5. Non-reacting simulations in terms of liquid and vapour penetration lengths and mixture fraction distribution are in acceptable agreement with the experiments and further reacting simulations can be conducted.

4.1.2. Reacting spray results

FGM table needs to be generated before starting the reactive Spray A simulations. As discussed the *n*-dodecane mechanism reduced by Yao *et al.* [38] is applied to generate flamelets using CHEM1D. Table 3 illustrates the FGM table generation parameters for Spray A reacting conditions. Simulation results were checked to possess minor dependency

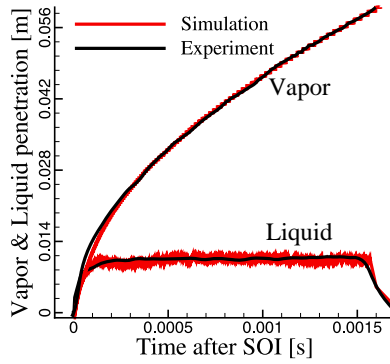


Figure 4. Non-reacting liquid and vapour penetration length comparison of the Spray A baseline case: 0% O_2 , 1500 bar injection pressure, 900 K ambient temperature, and 1.5 ms of injection duration (colour online).

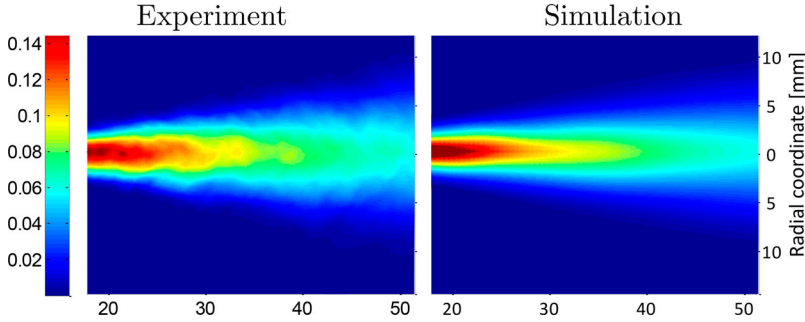


Figure 5. Spatial mixture fraction comparison of the non-reacting Spray A baseline case: 0% O_2 , 1500 bar injection pressure, 900 K ambient temperature at 0.75 ms (colour online).

Table 3. FGM table discretisation for modelling Spray A reacting conditions of 15% O_2 .

Parameter	Range	No. of discretisation points
Scaled progress variable	$0 < c < 1$	500
Mixture fraction	$0 < Z < 1$	500
Unburned temperature (K)	$750 < T_u < 1100$	6
Pressure (bar)	$50 < p < 80$	3

with the table grid resolutions of Table 3, where the goal was also keeping the table size as small as possible for storage and computational memory issues.

The solver discussed in Figure 1 uses the FGM table with the discretisation above and then reacting simulations can be conducted for baseline case (Table 1), 800 and 1000 K ambient temperature operating conditions. Results of ignition delay and flame lift-off for Spray A simulations for 800, 900, and 1000 K ambient temperatures are presented in Table 4. Ignition delay is the time delay between start of liquid fuel injection and start of self-sustaining and exothermic chemical reactions, whereas flame lift-off is characteristics for the high temperature combustion (diffusion combustion phase). The numerical

Table 4. Comparison of ignition delay and flame lift-off results of FGM combustion closure with ECN experiments of 800 K, 900 K, and 1000 K ambient temperatures.

Ambient temperature (K)	800	900	1000
Ignition delay (ms) simulation	0.91	0.45	0.25
<i>Experiment</i>	0.85	0.41	0.24
Flame lift-off (mm) simulation	25.1	16.5	11.7
<i>Experiment</i>	26.2	16.7	12.2

threshold for ignition time is based on ECN guidelines which is start of PRR for the diffusion combustion phase. Ignition delay time then is the time difference between SOI and ignition time. Flame lift-off was determined by the distance between injector orifice and the first location of Favre-average OH mass fraction reaching 2% of its maximum in the CFD domain during the simulation time.

It shows that by increasing ambient temperature ignition delay times shortens. This is due to accelerated fuel evaporation, mixing, and combustion in elevated temperatures. Numerical simulations were capable of mimicking such a trend with a good accuracy. Temporal validations were also shown in Figure 6 for PRR of the three ambient temperature cases. It also shows that developed numerical framework can comprehensively reproduce different phases of reacting *n*-dodecane spray combustion. For 900 and 1000 K ambient temperature conditions ignition delay times were well predicted but for 800 K case simulation tends to over predict it. This is mainly due to the applied chemical kinetics mechanism which was not validated for low temperature conditions. Developing more detailed *n*-dodecane chemical kinetics mechanisms is the topic of current research in the ECN community and there is a need to generate mechanisms with larger range of applicability. Results of Figure 6 when PRR plateaus (diffusion combustion phase) are well predicted for all ambient temperatures. At this times flame lift-off has been observed and measured in the experiments.

Spatial comparisons in terms of temperature and OH mass fraction contours for the different ambient temperatures are given in Figure 7. The experimental flame lift-off values are also marked for each of ambient temperature cases. Comparisons are made at 3 ms after SOI where all conditions are experiencing diffusion combustion. It should be noted that the minimum of temperature contours are scaled to the ambient temperature of the each case. It can be seen that simulated flame lift-off lengths are also in good agreement with the experiments. This is more interesting for the low temperature case of 800 K where most of former studies on Spray A literature failed to predict flame lift-off quantitatively.

After numerical implementation and its evaluation for different ambient temperatures of the Spray A experimental configuration, the following sections will focus on modelling combustion in light and heavy duty Diesel engines.

4.2. Light duty diesel engine experiments | ECN: spray B

4.2.1. Optical engine and diagnostic setup

The engine used for this study is the Sandia single cylinder optical Diesel operating under light duty conditions. The optical engine is designed so that the upper cylinder

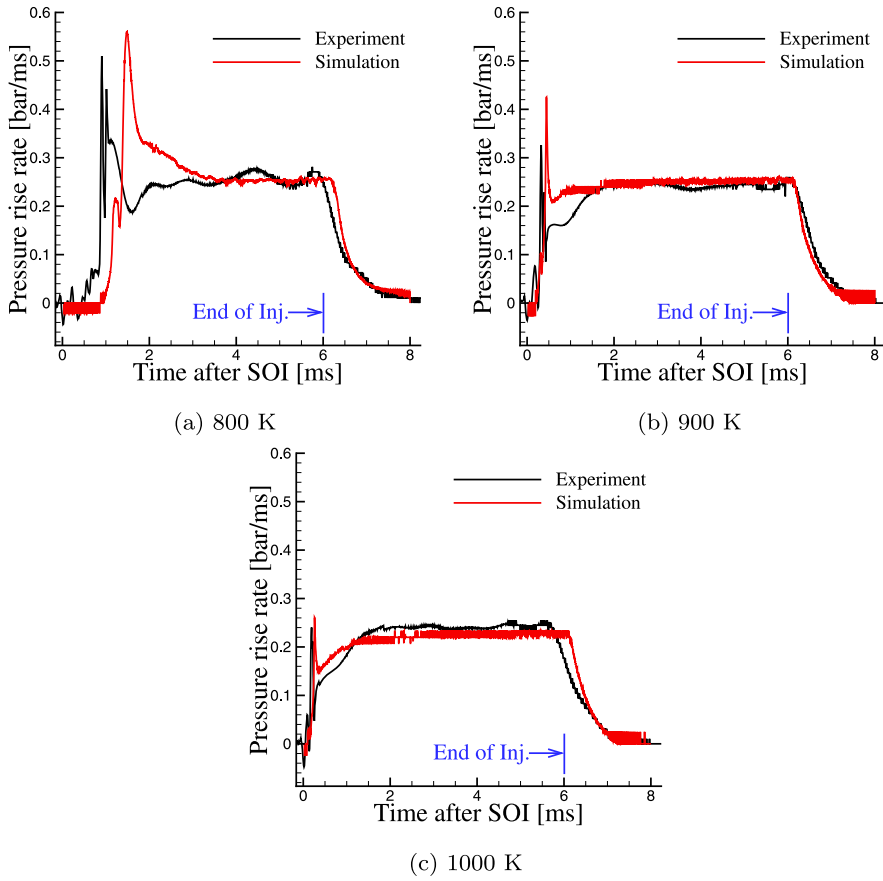


Figure 6. Temporal results of PRR for 800 900 and 100 K ambient temperatures compared with the experiments (colour online).

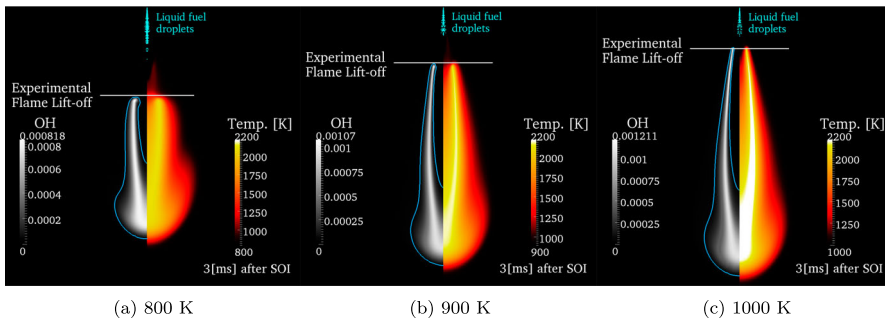


Figure 7. Temperature and OH mass fraction contours for Spray A ambient temperatures of 800, 900, and 1000 K with experimental flame lift-off lengths (colour online).

liner separates and drops down from the head without engine dis-assembly, for cleaning of in-cylinder optical surfaces. Experiments were conducted at Sandia National Labs. and for more information regarding the experiments refer to [41]. Selected details of the

Table 5. Sandia optical engine specifications [41].

Intake valves	2
Exhaust valves	1
Swirl ratio	0.5
Bore \times Stroke	13.97 \times 15.24 cm
Bowl width \times depth	9.78 \times 1.55 cm
Displacement	2.34 L
Compression ratio	11.22:1
Connecting rod length	30.48 cm

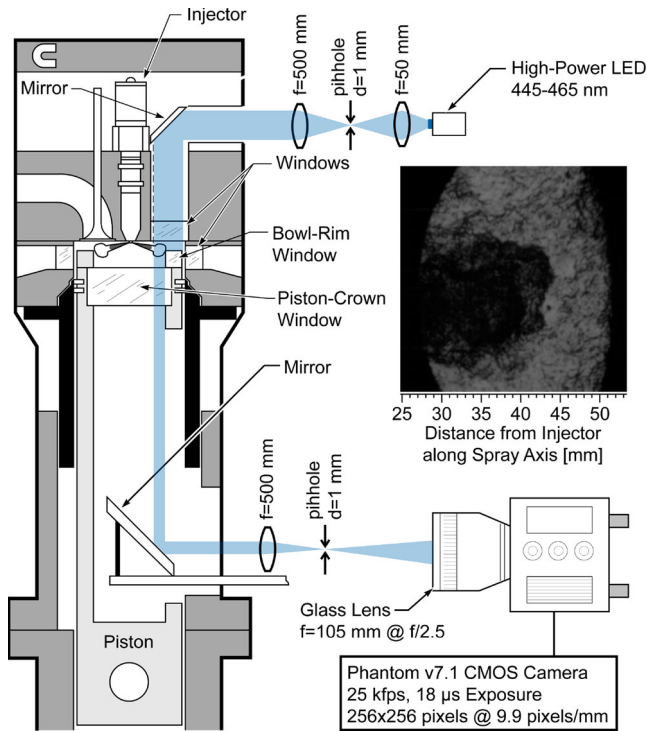


Figure 8. Extended-piston optical imaging schematic with the schlieren setup. Inset: Example instantaneous schlieren image at 364 CAD at ambient-gas conditions of 900 K, 15.2 kg/m^3 and 7.5% O_2 , with 1500 bar rail pressure [41] (colour online).

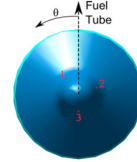
geometry for the engine appear in Table 5. The injector of interest is the ECN Spray B #211199, a three hole injector. Details of the injector are given in Table 6. In Figure 8, a schematic of the extended piston showing the optical path for the blue LED illumination and a monochrome Phantom v7.1 is used in a schlieren configuration for the detection of vapour penetration.

4.2.2. Engine mesh and boundary conditions

An automatic spray-oriented mesh generation tool which has been developed in previous studies [13,31] was used. Spray-oriented grid assures less numerical diffusion during the

Table 6. Sandia Spray B injector specifications.

Injector type	#211199 Bosch Spray B
Hole sizes, # ^{1,2,3}	90.9 μm , 91.7 μm , 90.9 μm
Nominal included angle	145°
Nozzle shaping	Smoothed
Discharge coefficient	$C_d = 0.86$
Hole angular position	# ¹ 36.4°, # ² - 62.3°, # ³ 180°



Notes: Orifice #³ was the orifice of interest in Spray B experiments. Bottom: Schematic orientation of the orifices for Spray B [2].

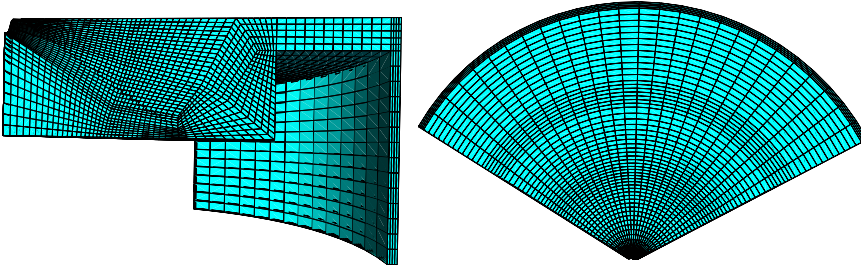


Figure 9. Spray-oriented grid automatically generated for Sandia optical engine Spray B experiments at TDC (colour online).

liquid fuel spray calculations if LDEF (Lagrangian Droplet and Eulerian Flow) method is applied [30]. Due to the configuration of the applied injector in Spray B experiments, spray-oriented grid is constructed for one-third of the Sandia optical engine. The grid size is 45,916 and 341,562 cells at TDC and BDC. The average cell size is less than 1 mm and tests were previously performed to verify grid-independent results [30]. Figure 9 shows the spray-oriented grid at TDC.

Multi-dimensional CFD simulations are conducted for the experimental conditions of Table 7. The 900 K case is referred to *Spray B*. Wall boundary layer treatment for heat transfer calculations is modelled by the Huh-Chang wall function [42]. Spray sub-models employed in this section were the same as in Spray A simulations of Section 4.1. Non-reactive and reactive engine simulations will be discussed next.

4.2.3. Non-reactive engine results

Experiments and numerical simulation results for the liquid and vapour penetration length of the Spray B cases are depicted in Figure 10. For the considered cases, only the 1000 K temperature liquid length is outside the standard deviation from the mean liquid length. Although within the measurement standard deviation, liquid penetration is systematically over-predicted. Vapour penetration mainly depends on the exchange of mass and

Table 7. Experimental initial conditions and properties of Spray B engine tests.

Case name	900 K	800 K	1000 K
Temperature at IVC (K)	380	340	454
Pressure at IVC (bar)	2.25	2.01	2.61
Temperature at TDC (K)	900	800	1000
Density at TDC (kg/m^3)		22.8	
Non-reacting O ₂ (%)	7.5	–	–
Reacting O ₂ (%)		15	
Injection pressure (bar)		1500	
Injected mass (mg/cycle)		3.68	
Engine Speed (rpm)		1200	
Inj. start (CAD ATDC)		–2.5	
Inj. duration (CAD)		11	

Note: 900 K case was named as *Spray B* for baseline engine case.

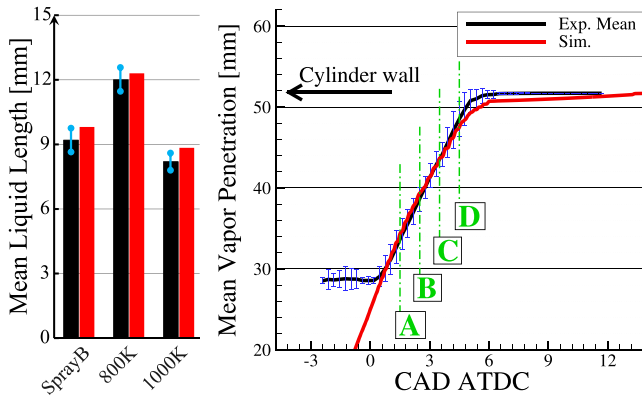


Figure 10. (Left) Mean liquid length (Red: Simulation, Black: Experiment) comparisons of the cases in Sandia optical engine. (Right) Temporal vapour penetration length of Spray B (baseline case) (colour online).

momentum between liquid and gas phase and is enhanced slightly by turbulent diffusivity. Figure 11 also compares spatial fuel vapour distribution and penetration values of the $Z = 0.001$ mixture fraction iso-surface in the numerical simulations compared to the experimental schlieren images at 1.5, 2.5, 3.5, and 4.5 CAD ATDC. These engine crank angles are also marked as A, B, C, and D in Figure 10. From both Figures 11 and 10 it can be concluded that numerical simulations are capable of acceptable predictions for vapour penetration and evaporated spray morphology compared to the experiments.

4.2.4. Frozen flamelet method

A 4D FGM table is needed for Spray B Diesel engine simulations. Chemical kinetics mechanism and FGM table discretisation for progress variable and mixture fraction were kept identical as in Table 3 except for unburned temperature and pressure. Compared to constant volume vessel, Diesel engine experiences larger ranges for the mentioned parameters and during the expansion stroke mean temperature drops to about 600 K. It is also possible

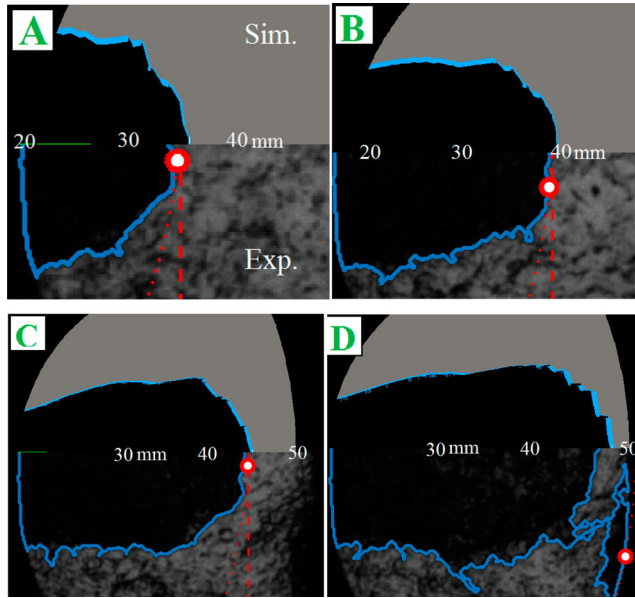


Figure 11. Spatial distribution of fuel vapour of the baseline case compared to experimental schlieren images for green **A**, **B**, **C**, and green **D** times in Figure 10 (colour online).

that charge composition contains some amount of unburned fuel with lower unburned temperature than 600 K at wall boundaries or piston crevice volume as well as burned gases after combustion. In such conditions, chemical reactivity of the mixture within combustion chamber is almost negligible due to the lowered temperature. From a modelling point of view, table generation should be performed for such conditions. For the Yao mechanism, HR flamelets can ignite from $T_u > 650$ K [21], whereas one dimensional counter flow flamelets may ignite from $T_u > 850$ K due to higher heat diffusion compared to HR flamelets. As mentioned for IC engine applications it is also necessary to have ignited and fully burned flamelet calculations (reaching to thermal equilibrium lines for all mixture fractions) at lowered temperatures. In such low temperatures, depending on the chemical kinetics mechanism, counter flow flamelets either do not ignite or it takes very long time to ignite and reach to equilibrium. It was mentioned that Lehtiniemi *et al.* [27] spent six month to create their flamelets for all ranges of unburned temperatures and pressures. This significantly hindered reliable application of tabulated chemistry within IC engine applications. In this work, FFM is introduced to enable generation of flamelets for mentioned low temperature conditions in acceptable computational times. The idea is to take an already ignited flamelet and apply new boundary condition for oxidiser temperature in a transient manner and keep it reacting and finally freeze it to mixing solution to determine intermediate thermal states and compositions. The FFM contains following procedure:

- (1) For each pressure interval the minimum T_u for igniting and fully burned transient flamelet was identified. Below this T_u there is either no ignition or it takes very long time to reach thermal equilibrium. It has been found that for oxidiser temperature above 850 K, *n*-dodecane can easily ignite and reach adiabatic flame temperature at stoichiometric mixture fraction. As shown in Figure 12 this is the first step.

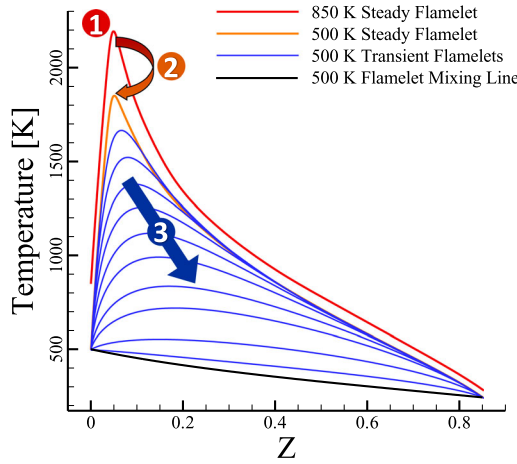


Figure 12. Schematic presentation of the FFM approach and steps to generate low temperature flamelets. (1) Identifying ignitable flamelet and taking its characteristics at thermal equilibrium, (2) Transient cooling down of the flamelet of the step 1 to a lower T_u and storing the final equilibrium, and (3) Transient freezing of the flamelet of the step 2 to the mixing solution and storing all transient flamelets (colour online).

- (2) The ignited flamelet solution at thermal equilibrium of the previous step was put as a initial condition for a new lower unburned temperature and flame is cooled down to the considered lower T_u . This is applied in a transient manner and boundary condition for oxidiser temperature of the burning flame was reduced from 850 K to say 500 K. It takes a short time for the oxidiser temperature to reduce to 500 K and to the flame to reach again to steady state condition but now for $T_u = 500$ K. This is the second step in Figure 12.
- (3) To fill the space between steady burning flame of the previous step and the mixing line a transient simulation is started where the chemistry is switched off and the flame gradually relaxes to the mixing solution. However, in this step data for all transient freezing flamelets, blue curves in Figure 12, were stored which later will be needed for generating FGM table. Within this step all thermal states and compositions of $T_u = 500$ K from steady-state burning flame to non-reactive mixing solution will be stored.
- (4) Repeating all mentioned steps for any lower value of T_u . Using the explained steps above, steady-state burning flamelets can be further cooled down to a lower oxidiser temperatures making extensive flamelet database for unburned temperatures in reasonable simulation times.

Using this method FGM tables for the Spray B simulations were generated. Progress variable and mixture fraction values are used as in Table 3 and $400 \text{ K} < T_u < 1300 \text{ K}$ with 50 K intervals for unburned temperature and five pressure values in range of $5 \text{ bar} < p < 70 \text{ bar}$ are applied. Table 8 summarises table sizes of Spray A and Spray B configurations and the time needed for flamelet and table generation.

It shows that time needed for table generation by applying FFM for IC engine application is not comparable to the six month time reported by Lehtiniemi *et al.* [27]. Using this FGM table it was possible to model ignition and combustion of the Spray B engine as well as

Table 8. Comparison of the table resolution and generation times for Spray A and Spray B configurations.

Configuration	Spray A	Spray B
Application	Constant volume vessel	Engine
FFM	Not applied	Applied for $T_u < 850 K$
c range, No. of points	$0 < c < 1, 500$	$0 < c < 1, 500$
Z range, No. of points	$0 < Z < 1, 500$	$0 < Z < 1, 500$
T_u (K) range, No. of points	$750 < T_u < 1100, 6$	$400 < T_u < 1300, 19$
p (bar) range, No. of points	$50 < p < 80, 3$	$5 < p < 70, 5$
Total time for flamelet and table generation (hrs)	1.9	11.2

its thermal state while expansion and at wall boundaries. The results of reactive engine simulations will be discussed next.

4.2.5. Reactive engine results

Reacting engine results for in-cylinder pressure and Apparent Heat Release Rate (AHRR) of the cases presented in Table 7 are discussed in Figure 13. It shows that numerical simulations can mimic experimental in-cylinder pressure and AHRR with a good accuracy. The premixed burning phase is more pronounced for 800 K case and tends to reduce when charge temperature is increased. For the low temperature case of 800 K numerical simulations result in earlier ignition (approximately 2 CAD) compared to the experiments. This can be attributed to the poor validation of the Yao mechanism at low temperatures. For higher temperatures mechanism was capable of accurate predictions for time of ignition and the AHRR during diffusion combustion and burnout phase.

Transient flame lift-off results are compared to the experimental values in Figure 14. The figure also shows simulated iso-surfaces of 2% of the maximum OH as a marker of the diffusion flame. It should be mentioned that the experimental mean flame lift-off values were determined during a small time duration when diffusion combustion was dominant [41]. Figure 14 shows that numerically larger flame lift-off values are obtained at the start of diffusion combustion and then as the time progresses flame lift-off becomes shorter. Iso-contours of 2% of the maximum OH show that by increasing the ambient temperature at SOI, flame lift-off becomes shorter. This is due to accelerated fuel evaporation and mixing as well as faster chemical heat release at higher temperatures.

4.3. Heavy duty diesel engine experiments | sandia optical engine

Prior to the Spray B experiments, Singh *et al.* used the same engine to perform heavy duty engine experiments [43]. The engine was operating under higher compression ratio of 16 and a larger amount of injected fuel. Table 9 represents the characteristics of two high temperature cases selected for further numerical validation. The intake temperature was varied to create two cases with *High Temperature Short Ignition Delay* (HT-Sh-ID) and *High Temperature Long Ignition Delay* (HT-Lo-ID). It can be seen that amount of injected mass for the depicted heavy duty operating condition of Table 9 were 16 times larger than Spray B engine experiments. Similar to the mesh in Figure 9 a sector spray-oriented grid was generated but for one-eighth of the combustion chamber as injector had eight orifices.

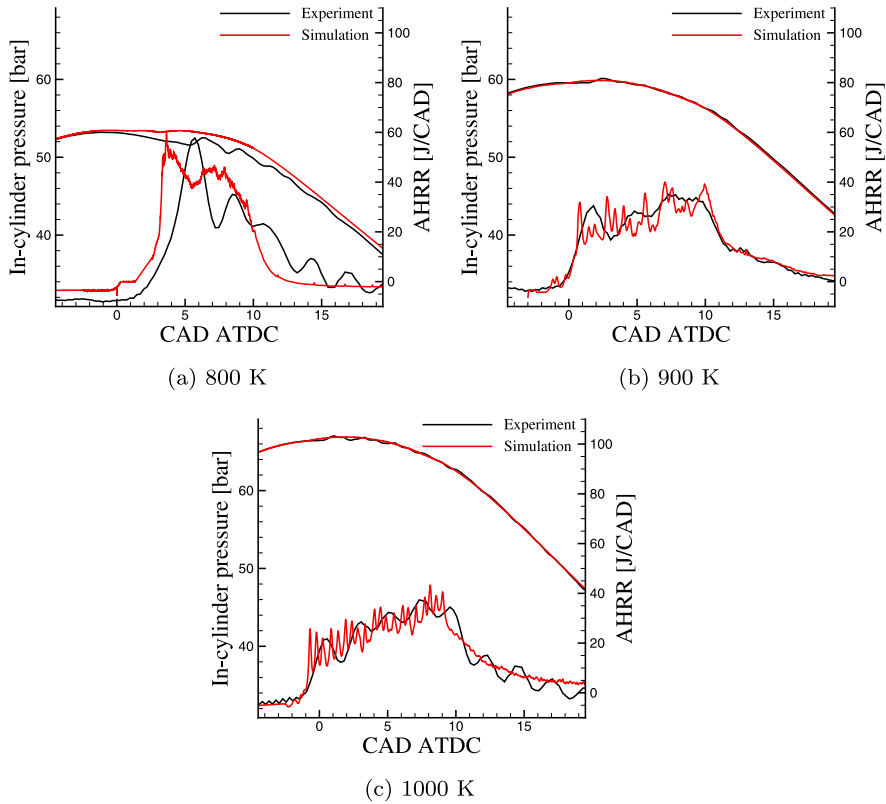


Figure 13. Temporal results of in-cylinder pressure and AHRR for 800 K, 900 K, and 1000 K compared with the experiments (colour online).

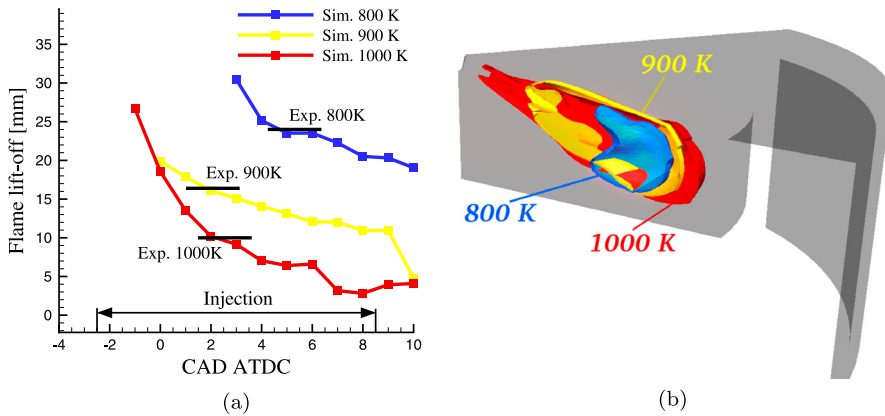


Figure 14. (a) Temporal results of flame lift-off for 800 K, 900 K, and 1000 K ambient temperatures compared with the mean experimental values. (b) Iso-surfaces 2% of the maximum OH as a marker of the diffusion flame at 5 CAD ATDC for targeted ambient temperatures (colour online).

Table 9. Specifications of Sanida engine under heavy duty operating condition [43].

Case	HT-Sh-ID	HT-Lo-ID
Engine speed (rpm)	1200	1200
Temperature at IVC (K)	384	320
Pressure at IVC (bar)	1.2	1.2
Temperature at TDC (K)	900	800
Density at TDC (kg/m^3)	24	22.3
Injected mass (mg/cycle)	61	61
Inj. start (CAD ATDC)	-7	-5
Inj. duration [CAD]	10	10
O ₂ concentration (% by Vol.)	21	21

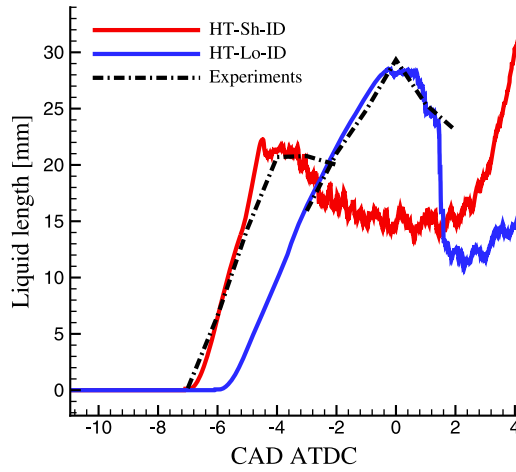


Figure 15. Temporal spray liquid length of the HT-Sh-ID and HT-Lo-ID cases compared with the experiments (colour online).

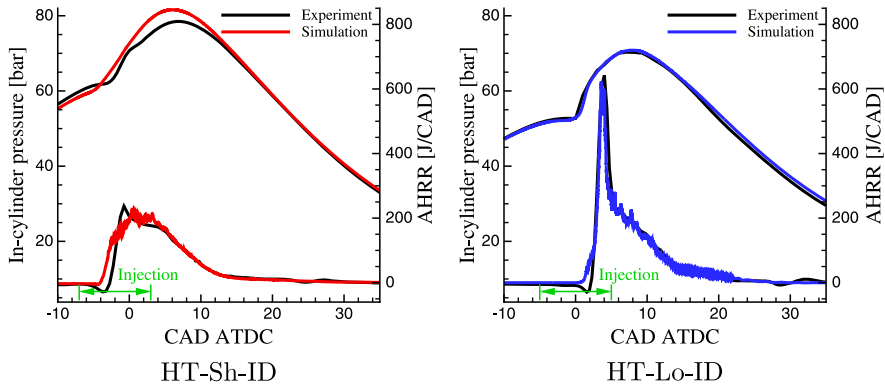


Figure 16. In-cylinder pressure and AHRR of the HT-Sh-ID and HT-Lo-ID cases compared with the experiments (colour online).

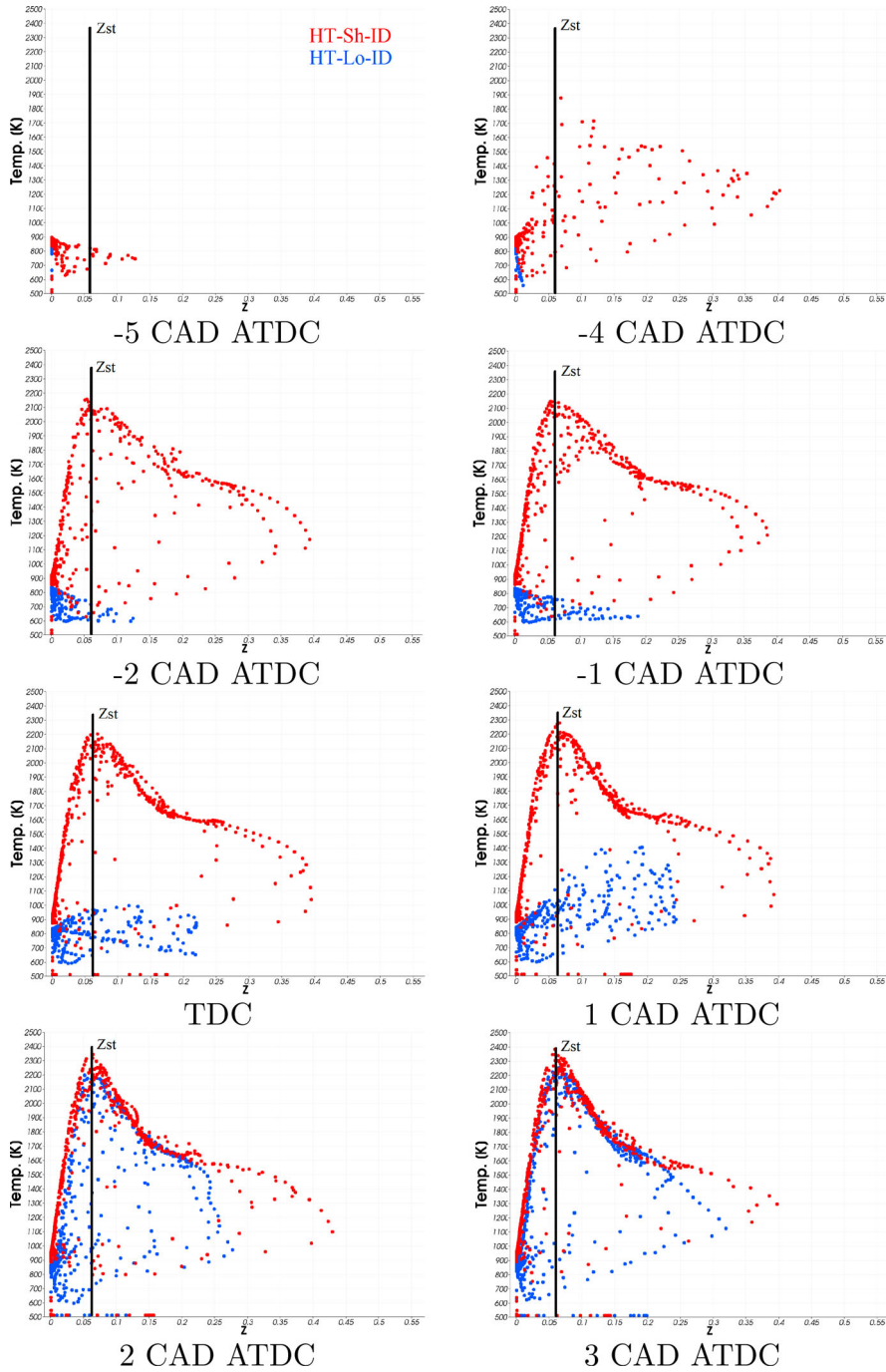


Figure 17. (a) Mixture fraction – Temperature flame structure diagrams for • HT-Sh-ID and • HT-Lo-ID cases at specified CADs (colour online).

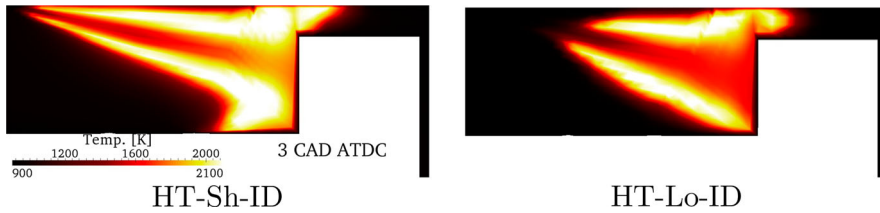


Figure 18. Temperature contour of the HT-Sh-ID and HT-Lo-ID cases during diffusion combustion at 3 CAD ATDC (colour online).

Figure 15 shows results of spray liquid length compared with experiments. Applied numerical sub-models for heavy duty spray simulations were identical to Spray B engine in Section 4.2.3. Liquid length results of the heavy duty simulation cases are in good agreement with the experiments. Note that for almost the same injection duration as Spray B, the amount of injected mass is 16 times higher. It can be seen that for the HT-Lo-ID case the liquid spray penetration is larger than that of HT-Sh-ID. This is due to lower ambient temperature and fuel evaporation for the HT-Lo-ID case.

For reacting simulations, 4D FGM tables were generated for 21% O_2 concentration using the FFM methodology described in Section 4.2.4. The same table resolution as Spray B was used for table generation parameters. For the heavy duty engine cases higher cylinder pressures occur, seven pressure levels were used in this case up to the maximum of 90 bar. Results of in-cylinder pressure and AHRR are presented in Figure 16. Compared to Spray B light duty engine, both heavy duty cases exhibit a considerable pressure rise and AHRR. Higher charge temperature in HT-Sh-ID case results in earlier ignition and chemical heat release, whereas for HT-Lo-ID case ignition started after TDC. Similar to Spray B, longer ignition delay results in intensified premixed burning phase. This is because of the accumulation of a larger amount of evaporated fuel during this phase. In both cases FGM method was able to predict peak pressure, AHRR magnitudes and timing well compared to the experiments.

In order to see how combustion progresses in the studied heavy duty cases, temperature scatters in mixture fraction space are presented in Figure 17. It shows that ignition was initiated at -4 CAD ATDC for the HT-Sh-ID case where temperature for a range of mixture fractions up to $Z = 0.4$ is elevated. Then reacting zone phases and reaches to diffusion combustion at 3 CAD ATDC. In HT-Lo-ID case, ignition occurs at 1 CAD ATDC where compared to the HT-Sh-ID case a narrower range of mixture fraction (maximum $Z = 0.25$) ignites. This is because of the lower ambient temperature which reduces the fuel evaporation and air-fuel mixing for HT-Lo-ID case. Both of the cases reach diffusive combustion at 3 CAD ATDC where the maximum burning temperature occurs at $Z_{St} = 0.062$. Temperature contours for 3 CAD ATDC are also shown in Figure 18. The flame exhibits a smaller lift-off for the HT-Sh-ID case and also the high temperature flame brush is wider than that of the HT-Lo-ID case. Both of these effects can be also explained with scatter plots in Figure 17 at 3 CAD ATDC. Higher reactivity of the HT-Sh-ID case in both lean and rich mixture fractions was result in a shortened flame lift-off and thickened reactive flame brush.

5. Conclusions

The application of the FGM combustion closure, source code, and model development on simulation of Diesel engines are presented. The developed numerical framework is used to

simulate Spray A, a constant volume vessel, Spray B, a light duty Diesel, and a heavy duty Diesel engine experiments. After evaluating numerical results for liquid spray modelling in terms of liquid length and vapour penetration, reacting simulations were conducted. Conclusions below can be made:

- (1) An extensive validation on constant volume vessel, light, and heavy duty Diesel engine characteristics of ignition delay, in-cylinder pressure, apparent heat release rate, and flame lift-off showed that FGM combustion closure is capable of accurate predictions for non/partially premixed combustion configuration under a variety of operating conditions.
- (2) FFM was introduced and successfully applied for FGM table generation at lower oxidiser temperatures where a flamelet fails to ignite in reasonable computational times. FFM enables a correct determination of the engine thermal state at expansion stroke.
- (3) For all configurations it was concluded that higher ambient temperatures at SOI result in lowered ignition delay times and shortened flame lift-off. Also less premixed burning rates were resulted for shorter ignition delay times and combustion was phased faster to diffusion phase.
- (4) Applied *n*-dodecane chemical kinetics mechanism of Yao *et al.* [38] performs well for ambient temperatures of 900 and 1000 K. However, the same level of accuracy is not observed for low ambient temperature of 800 K. There is a need to develop reduced *n*-dodecane mechanisms validated for a larger range of temperature, pressure, and equivalence ratio.

Disclosure statement

No potential conflict of interest was reported by the authors.

Funding

This work was supported by Nederlandse Organisatie voor Wetenschappelijk Onderzoek.

References

- [1] R.D. Reitz, *Directions in internal combustion engine research*, Combust. Flame 1(160) (2013), pp. 1–8.
- [2] Sandia Engine Combustion Network Database, 2018. Available at <http://www.ca.sandia.gov/ecn>.
- [3] L.M. Pickett, C.L. Genzale, G. Bruneaux, L-M. Malbec, L. Hermant, C.A. Christiansen, and J. Schramm, *Comparison of diesel spray combustion in different high-temperature, high-pressure facilities*, SAE Int. J. Eng. 3(2) (2010), pp. 156–181.
- [4] L.M. Pickett, J. Manin, C.L. Genzale, D.L. Siebers, M.P.B. Musculus, and C.A. Idicheria, *Relationship between diesel fuel spray vapor penetration/dispersion and local fuel mixture fraction*, SAE Int. J. Eng. 4 (2011), pp. 764–799, 2011-01-0686
- [5] L. Zhaoyu, S. Som, S.M. Sarathy, M. Plomer, W.J. Pitz, D.E. Longman, and T. Lu, *Development and validation of an n-dodecane skeletal mechanism for spray combustion applications*, Combust. Theory Model. 18(2) (2014), pp. 187–203.
- [6] Y. Pei, E.R. Hawkes, S. Kook, G.M. Goldin, and T. Lu, *Modeling n-dodecane spray and combustion with the transported probability density function method*, Combust. Flame 162(5) (2015), pp. 2006–2019.
- [7] F. Contino, H. Jeanmart, T. Lucchini, and G. D'Errico, *Coupling of in situ adaptive tabulation and dynamic adaptive chemistry: An effective method for solving combustion in engine simulations*, Proc. Combust. Inst. 33(2) (2011), pp. 3057–3064.

- [8] C.K. Westbrook, W.J. Pitz, O. Herbinet, H.J. Curran, and E.J. Silke, *A comprehensive detailed chemical kinetic reaction mechanism for combustion of n-alkane hydrocarbons from n-octane to n-hexadecane*, *Combust. Flame* 156(1) (2009), pp. 181–199.
- [9] C.J. Rutland, *Large-eddy simulations for internal combustion engines—a review*, *Int. J. Eng. Res.* 12(5) (2011), pp. 421–451.
- [10] L. Long, J.G. Stevens, and J.T. Farrell, *A dynamic adaptive chemistry scheme for reactive flow computations*, *Proc. Combust. Inst.* 32(1) (2009), pp. 527–534.
- [11] S.B. Pope, *Computationally efficient implementation of combustion chemistry using in-situ adaptive tabulation*, *Combust. Theory Model.* 1 (1997), pp. 14–63.
- [12] M.S. Aceves, D.L. Flowers, C.K. Westbrook, J.R. Smith, W. Pitz, R. Dibble, M. Christensen, and B. Johansson, *A multi-zone model for prediction of HCCI combustion and emissions*, SAE Paper 2000-01-0327, 2000.
- [13] A. Maghbouli, T. Lucchini, G. D’Errico, A. Onorati, L.-M. Malbec, M.P.B. Musculus, and W.E. Eagle, *Parametric comparison of well-mixed and flamelet n-dodecane spray combustion with engine experiments at well controlled boundary conditions*, SAE Paper 2016-01-0577, 2016.
- [14] M. Ihme, L. Shunn, and J. Zhang, *Regularization of reaction progress variable for application to flamelet-based combustion models*, *J. Comput. Phys.* 231(23) (2012), pp. 7715–7721.
- [15] J.A. van Oijen and L.P.H. de Goey, *Modeling of premixed laminar flames using flamelet-generated manifolds*, *Combust. Sci. Technol.* 161(1) (2000), pp. 113–137.
- [16] C. Bekdemir, L.M.T. Somers, and L.P.H. de Goey, *Modeling diesel engine combustion using pressure dependent Flamelet generated manifolds*, *Proc. Combust. Inst.* 33(2) (2011), pp. 2887–2894.
- [17] O. Gicquel, N. Darabiha, and D. Thevenin, *Laminar premixed hydrogen/air counterflow flame simulations using flame propagation of ILDM with differential diffusion*, *Proc. Combust. Inst.* 28 (2000), pp. 1901–1908.
- [18] C. Correa, H. Niemann, B. Schramm, and J. Warnatz, *Use of ILDM reduced chemistry in direct injection Diesel engines*, *Thermo- and Fluid-Dynamic Processes in Diesel Engines*, Selected Papers from the THIESEL 2000 Conference, pp. 353–362, 2002.
- [19] V. Fichet, *Modélisation de la combustion du gaz naturel par réseaux de reacteurs avec cinétique chimique détaillée*, PhD thesis, Ecole Centrale Paris, 2008.
- [20] F. Tap and P. Schapotschnikow, *Efficient combustion modeling based on Tabkin CFD look-up tables: A case study of a lifted diesel spray flame*, SAE Paper 2012-01-0152, 2012.
- [21] T. Lucchini, G. D’Errico, A. Onorati, A. Frassoldati, and A. Stagni, *Modeling non-premixed combustion using tabulated Kinetics and different fame structure assumptions*, *SAE Int. J. Eng.* 10 (2017), pp. 593–607, 2017-01-0556.
- [22] J.M. García-Oliver, R. Novella, J.M. Pastor, and J.F. Winklinger, *Evaluation of combustion models based on tabulated chemistry and presumed probability density function approach for diesel spray simulation*, *Int. J. Comput. Math.* 91(1) (2014), pp. 14–23.
- [23] S. Bhattacharjee and D.C. Haworth, *Simulations of transient n-heptane and n-dodecane spray flames under engine-relevant conditions using a transported PDF method*, *Combust. Flame* 160 (2013), pp. 2083–2102.
- [24] P. Kundu, Y. Pei, M. Wang, R. Mandhapaty, and S. Som, *Evaluation of turbulence-chemistry interaction under diesel engine conditions with multi-flamelet RIF model*, *Atomization Sprays* 24(9) (2014), pp. 779–800.
- [25] G. D’Errico, T. Lucchini, F. Contino, M. Jangi, and X.S. Bai, *Comparison of well-mixed and multiple representative interactive flamelet approaches for diesel spray combustion modeling*, *Combust. Theory Model.* 18 (2014), pp. 65–88.
- [26] A. Wehrfritz, O. Kaario, V. Vuorinen, and L.M.T. Somers, *Large Eddy simulation of n-dodecane spray flames using flamelet generated manifolds*, *Combust. Flame* 167 (2016), pp. 113–131.
- [27] H. Lehtiniemi, F. Mauss, M. Balthasar, and I. Magnusson, *Modeling diesel engine combustion with detailed chemistry using a progress variable approach*, SAE Paper 2005-01-3855, 2005.
- [28] U. Egüz, N. Leermakers, B. Somers, and P. de Goey, *Modeling of PCCI combustion with FGM tabulated chemistry*, *Fuel* 118 (2014), pp. 91–99.
- [29] P. Kundu, M. Ameen, U. Unnikrishnan, and S. Som, *Implementation of a tabulated flamelet model for compression ignition engine applications*, SAE Technical Paper 2017-01-0564, 2017.

- [30] A. Maghbouli, T. Lucchini, G. D'Errico, and A. Onorati, *Effects of grid alignment on modeling the spray and mixing process in direct injection diesel engines under non-reacting operating conditions*, Appl. Therm. Eng. 91 (2015), pp. 901–912.
- [31] A. Maghbouli, *Development of an advanced multi-dimensional CFD framework for modeling low temperature combustion in direct injection compression ignition engines*, PhD thesis, Politecnico di Milano, 2017.
- [32] N. Peters, *Laminar diffusion flamelet models in non-premixed turbulent combustion*, Prog. Energy Combust. Sci. 10 (1984), pp. 319–339.
- [33] U. Maas and S.B. Pope, *Simplifying chemical kinetics: Intrinsic low-dimensional manifolds in composition space*, Combust. Flame 88(3) (1992), pp. 239–264.
- [34] G. Stahl and J. Warnatz, *Numerical investigation of time-dependent properties and extinction of strained methane and propane-air flamelets*, Combust. Flame 85(3–4) (1991), pp. 285–299.
- [35] L.M.T. Somers, *The simulation of flat flames with detailed and reduced chemical models*, PhD thesis, Eindhoven University of Technology, 1994.
- [36] CHEM1D, *One-dimensional laminar flame code*, Eindhoven University of Technology. Available at <http://www.combustion.tue.nl/chem1d>.
- [37] G. D'Errico, T. Lucchini, and A. Onorati, *Computational fluid dynamics modeling of combustion in heavy-duty diesel engines*, Int. J. Eng. Res. 16(1) (2015), pp. 112–124.
- [38] T. Yao, Y. Pei, B.J. Zhong, S. Som, and T. Lu, *A hybrid mechanism for n-dodecane combustion with optimized low-temperature chemistry*, 9th US National Combustion Meeting, Cincinnati, OH, 2015.
- [39] C. Bekdemir, L.M.T. Somers, L.P.H. De Goey, J. Tillou, and C. Angelberger, *Predicting diesel combustion characteristics with large-eddy simulations including tabulated chemical kinetics*, Proc. Combust. Inst. 34(2) (2013), pp. 3067–3074.
- [40] S. Ayyapureddi, U. Eguz, C. Bekdemir, B. Somers, and P. De Goey, *Application of the FGM Method to Spray A Conditions of the ECN database*, 12th Triennial international conference on liquid atomization and spray systems (ICLASS 2012), Heidelberg, Germany, 2012.
- [41] W.E. Eagle, L.-M. Malbec and M.P.B. Musculus, *Measurements of liquid length, vapor penetration, ignition delay, and flame lift-off length for the engine combustion network 'Spray B' in a 2.34 L heavy-duty optical diesel engine*, SAE Int. J. Eng. 9 (2016), pp. 910–931, 2016-01-0743.
- [42] K.Y. Huh, I.P. Chang and J.K. Martin, *A comparison of boundary layer treatments for heat transfer in IC engines*, SAE Paper 900252, 1990.
- [43] S. Singh, R.D. Reitz and M.P.B. Musculus, *Comparison of the characteristic time (CTC), representative interactive flamelet (RIF), and direct integration with detailed chemistry combustion models against optical diagnostic data for multi-mode combustion in a heavy-duty DI diesel engine*, SAE Paper 2006-01-0055, 2006.